Targeting of Lectinlike Oxidized Low-Density Lipoprotein Receptor 1 (LOX-1) with ^{99m}Tc-Labeled Anti–LOX-1 Antibody: Potential Agent for Imaging of Vulnerable Plaque

Seigo Ishino[1], Takahiro Mukai[2], Yuji Kuge[1], Noriaki Kume[3], Mikako Ogawa[4], Nozomi Takai[1], Junko Kamihashi[1], Masashi Shiomi[5], Manabu Minami[3], Toru Kita[3], and Hideo Saji[1]

[1]Department of Patho-Functional Bioanalysis, Graduate School of Pharmaceutical Sciences, Kyoto University, Kyoto, Japan; [2]Department of Biomolecular Recognition Chemistry, Graduate School of Pharmaceutical Sciences, Kyushu University, Fukuoka, Japan; [3]Department of Cardiovascular Medicine, Graduate School of Medicine, Kyoto University, Kyoto, Japan; [4]Laboratory of Genome Bio-Photonics Photon Medical Research Center, Hamamatsu University School of Medicine, Hamamatsu, Japan; and [5]Institute for Experimental Animals, Kobe University School of Medicine, Kobe, Japan

Lectinlike oxidized low-density lipoprotein (LDL) receptor 1 (LOX-1), a cell surface receptor for oxidized LDL, has been implicated in vascular cell dysfunction related to plaque instability, which could be a potential target for an atherosclerosis imaging tracer. In this study, we designed and prepared ^{99m}Tc-labeled anti–LOX-1 monoclonal IgG and investigated its usefulness as an atherosclerosis imaging agent. **Methods:** Anti–LOX-1 monoclonal IgG and control mouse IgG2a were labeled with ^{99m}Tc after derivatization with 6-hydrazinonicotinic acid to yield ^{99m}Tc-LOX-1-mAb and ^{99m}Tc-IgG2a, respectively. Myocardial infarction–prone Watanabe heritable hyperlipidemic (WHHLMI) rabbits (atherosclerosis model) and control rabbits were injected intravenously with these probes, and in vivo planar imaging was performed. At 24 h after the injection, the aortas were removed, and radioactivity was measured. Autoradiography and histologic studies were performed with serial aortic sections. **Results:** The level of ^{99m}Tc-LOX-1-mAb accumulation was 2.0-fold higher than the level of ^{99m}Tc-IgG2a accumulation in WHHLMI rabbit aortas, and the level of ^{99m}Tc-LOX-1-mAb accumulation in WHHLMI rabbit aortas was 10.0-fold higher than the level of ^{99m}Tc-LOX-1-mAb accumulation in control rabbit aortas. In vivo imaging clearly visualized the atherosclerotic aortas of WHHLMI rabbits. Autoradiography and histologic studies revealed that regional ^{99m}Tc-IgG2a accumulation was independent of the histologic grade of the lesions; however, regional ^{99m}Tc-LOX-1-mAb accumulation was significantly correlated with LOX-1 expression density and the vulnerability index. The highest level of ^{99m}Tc-LOX-1-mAb accumulation, expressed as {radioactivity in region of interest (Bq/mm^2)/[injected radioactivity (Bq)/animal body weight (g)]} $\times$ 10^2, was found in atheromatous lesions (3.8 $\pm$ 1.1 [mean $\pm$ SD]), followed in decreasing order by fibroatheromatous lesions (2.0 $\pm$ 1.0), collagen-rich lesions (1.6 $\pm$ 0.8), and neointimal lesions (1.4 $\pm$ 0.7). **Conclusion:** The level of ^{99m}Tc-LOX-1-mAb accumulation in grade IV atheroma was higher than that in neointimal lesions or other, more stable lesions. Nuclear imaging of LOX-1 expression with ^{99m}Tc-LOX-1-mAb may be a useful means for predicting atheroma at high risk for rupture.

Key Words: plaque; receptor; antibody; imaging; atherosclerosis

J Nucl Med 2008; 49:1677–1685
DOI: 10.2967/jnumed.107.049536

The spontaneous rupture of vulnerable atherosclerotic plaques and subsequent thrombus formation are currently recognized as the primary mechanisms of myocardial and cerebral infarctions (*1–3*). Evaluation of the vulnerability of atherosclerotic lesions is therefore clinically important for stratifying risk and providing early treatment. At present, however, no noninvasive diagnostic tools for the evaluation of plaque vulnerability are available for routine clinical use. Accordingly, the development of such noninvasive tools is urgently required.

Oxidized low-density lipoprotein (LDL) has been implicated in the pathogenesis of atherosclerosis and atherosclerotic plaque rupture by promoting lipid accumulation and vascular dysfunction. Lectinlike oxidized LDL receptor 1 (LOX-1) mediates the biologic effects of oxidized LDL in this process (*4*). Studies with cultured cells have suggested that LOX-1 may play several important roles in the destabilization of atherosclerotic plaques (*5–9*). Furthermore, our recent animal study indicated that LOX-1 expression in atherosclerotic plaques was positively correlated with plaque instability in vivo (*10*). Accordingly, the detection of LOX-1 expression may help assess the vulnerability of atherosclerotic plaques.

Nuclear medicine imaging enables the visualization of specific molecular processes in vivo and could be used for

Received Dec. 2, 2007; revision accepted Jun. 2, 2008.
For correspondence or reprints contact: Hideo Saji, Department of Patho-Functional Bioanalysis, Graduate School of Pharmaceutical Sciences, Kyoto University, Yoshida Shimoadachi-cho, Sakyo-ku, Kyoto 606-8501, Japan.
E-mail: hsaji@pharm.kyoto-u.ac.jp

imaging of the in vivo biologic properties of atherosclerotic plaques beyond morphologic information (*11,12*). The development of radiopharmaceuticals for the evaluation of plaque vulnerability is a matter of great concern in the clinical diagnosis of atherosclerosis.

In this study, we designed and prepared ^{99m}Tc-labeled anti–LOX-1 monoclonal IgG (^{99m}Tc-LOX-1-mAb) for investigation as an atherosclerosis imaging agent and ^{99m}Tc-labeled control mouse IgG2a (^{99m}Tc-IgG2a) for use as a control probe. Using an atherosclerosis model (myocardial infarction–prone Watanabe heritable hyperlipidemic [WHHLMI] rabbits) (*13*), we compared the accumulation of ^{99m}Tc-LOX-1-mAb and ^{99m}Tc-IgG2a in atherosclerotic lesions with histologic characteristics. Using these data, we evaluated the usefulness of ^{99m}Tc-LOX-1-mAb as an atherosclerosis imaging agent.

MATERIALS AND METHODS

Design and Preparation of ^{99m}Tc-LOX-1-mAb and ^{99m}Tc-IgG2a

A monoclonal antibody for rabbit LOX-1 (mouse IgG2a subtype) was established by use of a standard hybridoma technique (*10,14*). ^{99m}Tc-pertechnetate ($^{99m}TcO_4^-$) from Daiichi Radioisotope Laboratory generators was eluted in saline solution on a daily basis.

Anti–LOX-1 monoclonal IgG (LOX-1-mAb) was radiolabeled with ^{99m}Tc (^{99m}Tc-LOX-1-mAb) after derivatization with 6-hydrazinonicotinic acid (HYNIC) (*15*) according to a previously reported procedure (*16*) with slight modifications. In brief, HYNIC-*N*-hydroxysuccinimide was reacted with LOX-1-mAb, and the mixture was purified by size exclusion chromatography (Sephadex G-50 Fine; Amersham Pharmacia Biotech). To the purified solution of HYNIC–LOX-1-mAb was added an equal volume of ^{99m}Tc-$(tricine)_2$, prepared by the method of Larsen et al. (*17*), to obtain ^{99m}Tc-LOX-1-mAb. After purification of ^{99m}Tc-LOX-1-mAb by centrifugation of a size exclusion column with Sephadex G-50 Fine, the radiochemical purity of ^{99m}Tc-LOX-1-mAb was determined by cellulose acetate electrophoresis (Separax; Joko Co. Ltd.) to be 95.4% ± 2.2% (mean ± SD).

For the control study, negative control mouse IgG2a (Medical & Biologic Laboratories Co. Ltd.) was used for the preparation of ^{99m}Tc-IgG2a [with HYNIC and $(tricine)_2$]. The radiochemical purity of ^{99m}Tc-mouse IgG2a was 97.5% ± 0.9%.

Animal Preparation

All experimental procedures were approved by the Kyoto University Animal Care Committee. Three New Zealand White (NZW) rabbits (male, 3 mo old; Biotec, Inc.) were used to obtain peritoneal macrophages. For ^{99m}Tc-LOX-1-mAb biodistribution studies, 8 WHHLMI rabbits (5 male and 3 female, 11–24 mo old, 3.2 ± 0.5 kg; supplied by the Institute for Experimental Animals, Kobe University School of Medicine) were used. Six NZW rabbits (4 male and 2 female, 3.0 ± 0.3 mo old, 2.6 ± 0.5 kg; Biotec, Inc.) were used for the control study. For ^{99m}Tc-IgG2a biodistribution studies, 3 WHHLMI rabbits (2 male and 1 female, 11–13 mo old, 2.8 ± 0.2 kg) were used. The animals were fed standard chow (type CR-3; Clea Japan Inc.) at 120 g/d and were given water ad libitum.

Immunoreactivity of HYNIC–LOX-1-mAb

Rabbit peritoneal macrophages were obtained by the method of Ishii et al. (*18*) with minor modifications. The cells were suspended in medium A (Dulbecco's modified Eagle's medium containing 1 mM glutamine, penicillin at 100 U/mL, and streptomycin at 100 μg/mL [pH 7.4] as well as 0.2% lactalbumin hydrolysate) at a final concentration of 2.5×10^6 cells/mL. Aliquots of this cell suspension were placed in plastic petri dishes and then cultured in a humidified 5% CO_2 incubator at 37°C. After 2 h, each dish was washed twice with 10 mL of medium A to remove nonadherent cells. The monolayers were cultured for 18 h at 37°C in 20 mL of medium A, and the cells were washed twice with 10 mL of medium A and then used for experiments. More than 95% of the cells were viable, as determined by the trypan blue exclusion test, and almost all of the attached cells showed positive nonspecific esterase staining.

After the macrophages were stimulated for 6 h at 37°C in 5% CO_2 with tumor necrosis factor α at 10 ng/mL (Sigma-Aldrich, Inc.), the cells (10^6) were incubated with LOX-1-mAb (5 μg/mL, 100 μL), HYNIC–LOX-1-mAb (5 μg/mL, 100 μL), or control mouse IgG2a (5 μg/mL, 100 μL) for 30 min at 4°C. This step was followed by washing and incubation with Alexa Fluor 488 goat antimouse IgG (10 μg/mL, 100 μL; Molecular Probes, Inc.) for 30 min at 4°C. For flow cytometry analysis, cells were mixed with Iso-Flow solution (Beckman Coulter Inc.) and immediately analyzed with a FACScan instrument (Becton Dickinson Inc.). Data were analyzed with FACS software (BD CellQuest Pro; BD Biosciences Inc.). The immunoreactivity of HYNIC–LOX-1-mAb was evaluated on the basis of the median fluorescence intensity relative to that of control mouse IgG2a which, in turn, was compared with that of LOX-1-mAb. The measurements were obtained 3 times with rabbit peritoneal macrophages from 3 NZW rabbits, and the ratios were expressed as mean ± SD.

Noninvasive Imaging

After 12 h of fasting, rabbits were initially anesthetized with ketamine (7 mg/kg, intramuscularly) and xylazine (1 mg/kg, intramuscularly). The anesthetic state was maintained with additional doses of ketamine and xylazine during the experimental period. The rabbits were placed on the scanner bed in the prone position to include the abdominal aorta in the field of view. ^{99m}Tc-LOX-1-mAb (1,004 ± 110 MBq, 300 μg) or ^{99m}Tc-IgG2a (733 ± 44 MBq, 300 μg) was injected into a marginal ear vein of the rabbits (3 WHHLMI rabbits and 3 control rabbits for the ^{99m}Tc-LOX-1-mAb study and 3 WHHLMI rabbits for the ^{99m}Tc-IgG2a study). At 10 min and 24 h after injection of the radiotracer, planar images were obtained for 10 min by use of a SPECT-2000H scanner (Hitachi Medical Co.) with a low-energy, high-resolution, parallel-hole collimator having a spatial resolution of 6.7 mm at full width at half maximum. Arterial blood samples were collected from an auricular artery at 24 h. All rabbits were also used in biodistribution studies.

Biodistribution Studies

After rabbits had fasted for 12 h, ^{99m}Tc-LOX-1-mAb (122 ± 65 MBq, 300 μg) or ^{99m}Tc-IgG2a was injected into a marginal ear vein of the rabbits (8 WHHLMI rabbits and 6 control rabbits for the ^{99m}Tc-LOX-1-mAb study and 3 WHHLMI rabbits for the ^{99m}Tc-IgG study). At 24 h after the injection, all of the animals were sacrificed with an overdose of pentobarbital after blood sampling. The ascending aortic arch, the thoracic aorta, the abdominal aorta, the heart, and some femoral muscle were removed. The ascending aortic arch and thoracic and abdominal aortas were cut into 1-cm

segments. Each segment was weighed and immediately fixed in a solution containing L-(+)-lysine hydrochloride (75 mM) and 4% paraformaldehyde in phosphate buffer (37.5 mM, pH 7.4) (*19*). The radioactivity in each sample was measured with a well-type γ-counter (ARC-2000; Aloka). The results were expressed as the differential uptake ratio (DUR), which was calculated as (tissue activity/tissue weight)/(injected radiotracer activity/animal body weight), with activities given in becquerels and weights given in grams. The aorta-to-blood ratio (A/B ratio) and the aorta-to-muscle ratio (A/M ratio) were calculated from the DUR for each tissue sample.

Autoradiography (ARG) Studies

A total of 8 segments, the second and fifth segments of the ascending aortic arch and the second, fifth, and eighth segments each of the thoracic and abdominal aortas, from each animal were used for ARG studies. These segments were frozen and cut into 20-μm-thick slices with a cryomicrotome. The sections were thawed and mounted on silane-coated slides, which were then placed on a phosphorimaging plate (Fuji Imaging Plate BAS-UR; Fuji Photo Film) for 24 h together with a calibrated standard ($^{99m}TcO_4^-$ solution) to obtain ^{99m}Tc-LOX-1-mAb autoradiograms. The ARG images were analyzed by use of a computerized imaging analysis system (Bio Imaging Analyzer BAS3000 and Image Gauge Software; Fuji Photo Film). The radioactivity in each region of interest (ROI) was expressed as {radioactivity in ROI (Bq/mm^2)/[injected radioactivity (Bq)/animal body weight (g)]} × 10^2.

Histologic Analysis

The tissue sections used for ARG studies were also subjected to Azan–Mallory staining and hematoxylin–eosin (HE) staining. Therefore, ARG images were coincident with Azan–Mallory and HE images. Serial sections of the slices from the ARG studies were subjected to immunohistochemical staining (for LOX-1, macrophages, and smooth muscle cells). LOX-1 immunohistochemical staining was performed with LOX-1-mAb and an Envision+ kit (Dako) with hematoxylin counterstaining. In the same manner, immunohistochemical staining for macrophages and smooth muscle cells was performed with rabbit macrophage–specific monoclonal antibody RAM-11 (Dako) and human smooth muscle actin–specific monoclonal antibody 1A4 (Dako), respectively. Immunostaining with subclass-matched irrelevant IgG served as a negative control. Azan–Mallory staining and HE staining were performed by standard procedures. LOX-1 expression density was determined as a percentage of the positively stained region by use of a VHX digital microscope (Keyence Corp.).

To evaluate the correlation of ^{99m}Tc-LOX-1-mAb accumulation with LOX-1 expression density (Fig. 1), we divided each ARG image into 4 ROIs with vertical and horizontal lines as depicted in Figure 2B (dotted line) and then transferred the ROIs to the corresponding immunohistologic image (Fig. 2D, dotted line).

Definition of Atherosclerotic Lesions

Atherosclerotic lesions in WHHLMI rabbit aortas were divided into 4 categories by use of a classification scheme based on the recommendations of the American Heart Association (AHA) (*20,21*) and involving Azan–Mallory staining and HE staining as previously described (*22*): neointimal lesions (types I–III), atheromatous lesions (type IV), fibroatheromatous lesions (types Va and Vb), and collagen-rich lesions (type Vc) (Figs. 3 and 4).

Neointimal lesions (n = 28 for ^{99m}Tc-LOX-1-mAb study and n = 7 for ^{99m}Tc-IgG2a study) were defined as having adaptive thickening of the intima consisting of mainly smooth muscle cells and few macrophages. Atheromatous lesions (n = 46 and n = 20, respectively) contained thin fibrous connective tissue and a dense accumulation of extracellular lipid and foam cells and might correspond to apparently vulnerable lesions in human atherosclerotic plaques.

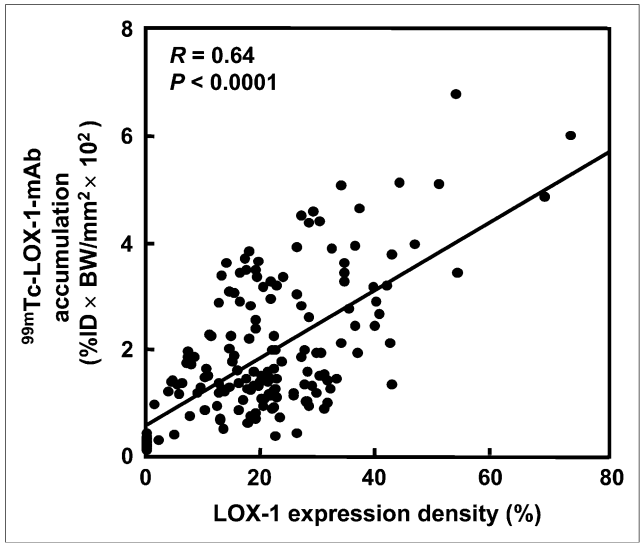

FIGURE 1. Correlation between ^{99m}Tc-LOX-1-mAb accumulation and LOX-1 expression density. Quantitative analysis of autoradiograms provided ^{99m}Tc-LOX-1-mAb accumulation, expressed as {radioactivity in ROI (Bq/mm^2)/[injected radioactivity (Bq)/animal body weight (g)]} × 10^2 (%ID × BW/mm^2 × 10^2).

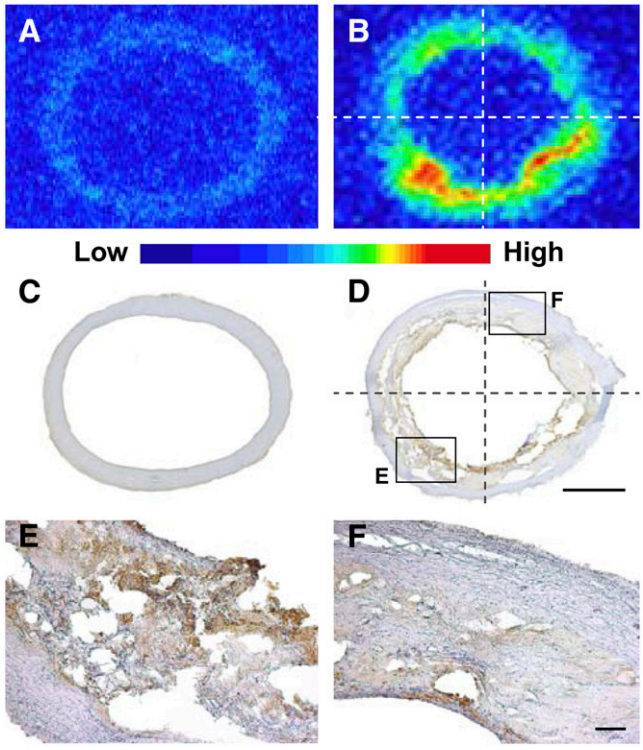

FIGURE 2. Regional distribution of ^{99m}Tc-LOX-1-mAb and LOX-1 expression in aortic sections. (A–D) Autoradiograms (A and B) and LOX-1 immunohistochemical staining (C and D) of control (A and C) and WHHLMI (B and D) rabbits. (E and F) High-magnification images of LOX-1 immunohistochemical staining from insets in D. Bars = 1 mm (C and D) and 100 μm (E and F).

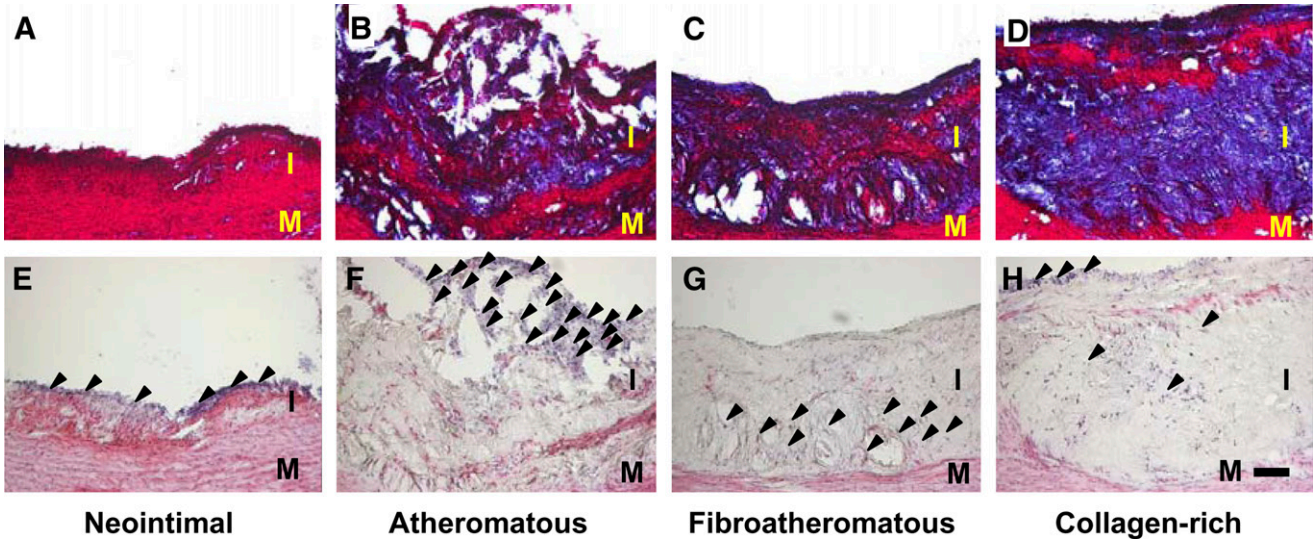

FIGURE 3. Representative photomicrographs of lesion types assigned with AHA classification scheme. (A–D) Azan–Mallory staining. (E–H) HE staining. Arrowheads mark inflammatory cell nuclei. I = intima; M = media. Bar = 100 μm.

Fibroatheromatous lesions ($n = 45$ and $n = 17$, respectively) were composed of several lipid cores separated by thick layers of fibromuscular connective tissue and might be stable against rupture (*23–25*). Collagen-rich lesions ($n = 73$ and $n = 49$, respectively) consisted of a predominantly collagenous component and contained smooth muscle cells. No lesions showed hemorrhage, plaque rupture, or thrombosis (type VI).

ROIs were placed over the atherosclerotic lesions in the WHHLMI rabbit aortic sections with reference to the classification scheme based on the Azan–Mallory and HE staining images and then were transferred to the corresponding ARG images.

Vulnerability Index

An index of morphologic destabilization characteristics, the vulnerability index, was calculated for each lesion in the WHHLMI rabbits by the method of Shiomi et al. (*26*) The vulnerability index was defined as the ratio of the lipid component area (macrophages and extracellular lipid deposits) to the fibromuscular component area (smooth muscle cells and collagen fibers). Collagen fibers and extracellular lipid deposits (extracellular vacuoles and lacunae) were determined with Azan–Mallory staining. Macrophages and smooth muscle cells were determined with immunohistochemical staining (RAM-11 and 1A4).

Statistical Analysis

Data are presented as mean ± SD. Statistical analysis was performed by use of the Mann–Whitney *U* test to compare aortic segments in WHHLMI and control rabbits (Table 1). Correlation coefficients were assessed by use of Spearman rank analysis (Figs. 1 and 5). Comparisons among lesion types were performed by use of the Kruskal–Wallis test, and post hoc analysis was performed by use of the Scheffe test (Fig. 6). A *P* value (2-tailed) of less than 0.05 was considered statistically significant.

RESULTS

Immunoreactivity of HYNIC–LOX-1-mAb

The median fluorescence intensity ratios for LOX-1-mAb and HYNIC–LOX-1-mAb relative to control mouse IgG2a were 1.63 ± 0.08 and 1.52 ± 0.11, respectively, indicating that the immunoreactivity of HYNIC–LOX-1-mAb was 93% that of LOX-1-mAb.

Noninvasive Imaging

The planar images showed primarily blood-pool radioactivity in the abdominal aorta at 10 min after the injection of ^{99m}Tc-LOX-1-mAb or ^{99m}Tc-IgG2a into WHHLMI and control rabbits (Figs. 7A–7C). At 24 h, with decreased blood-pool radioactivity in the abdominal aorta, the atherosclerotic abdominal aorta with ^{99m}Tc-LOX-1-mAb was more clearly visible than the control aorta with ^{99m}Tc-LOX-1-mAb or the atherosclerotic aorta with ^{99m}Tc-IgG2a (Figs. 7D–7F).

Biodistribution Studies

The distributions of ^{99m}Tc-LOX-1-mAb and ^{99m}Tc-IgG2a in the aortic segments of WHHLMI and control rabbits are summarized in Table 1. The level of ^{99m}Tc-LOX-1-mAb accumulation in each aortic segment in WHHLMI rabbits was 7.9- to 12.1-fold higher than that in control rabbits, and the differences were significant. A significant difference in ^{99m}Tc-LOX-1-mAb accumulation was not observed between young WHHLMI rabbits (11–13 mo) and old WHHLMI rabbits (20–24 mo) (DURs of 3.3 ± 1.4 and 2.8 ± 2.1, respectively). Blood-pool radioactivity levels (DURs) at 24 h were 4.5 ± 0.5 and 3.5 ± 0.4 in WHHLMI and control rabbits, respectively. A/B and A/M ratios were significantly higher in WHHLMI rabbits than in control rabbits. Relatively high levels of ^{99m}Tc-LOX-1-mAb accumulation were found in the liver, spleen, and kidneys in both groups of rabbits (data not shown). No marked difference in the distribution of ^{99m}Tc-LOX-1-mAb in nontarget organs was observed between WHHLMI and control rabbits.

The level of ^{99m}Tc-LOX-1-mAb accumulation in WHHLMI rabbit aortas was 1.8- to 2.5-fold higher than the level of ^{99m}Tc-IgG2a accumulation, and the differences were significant.

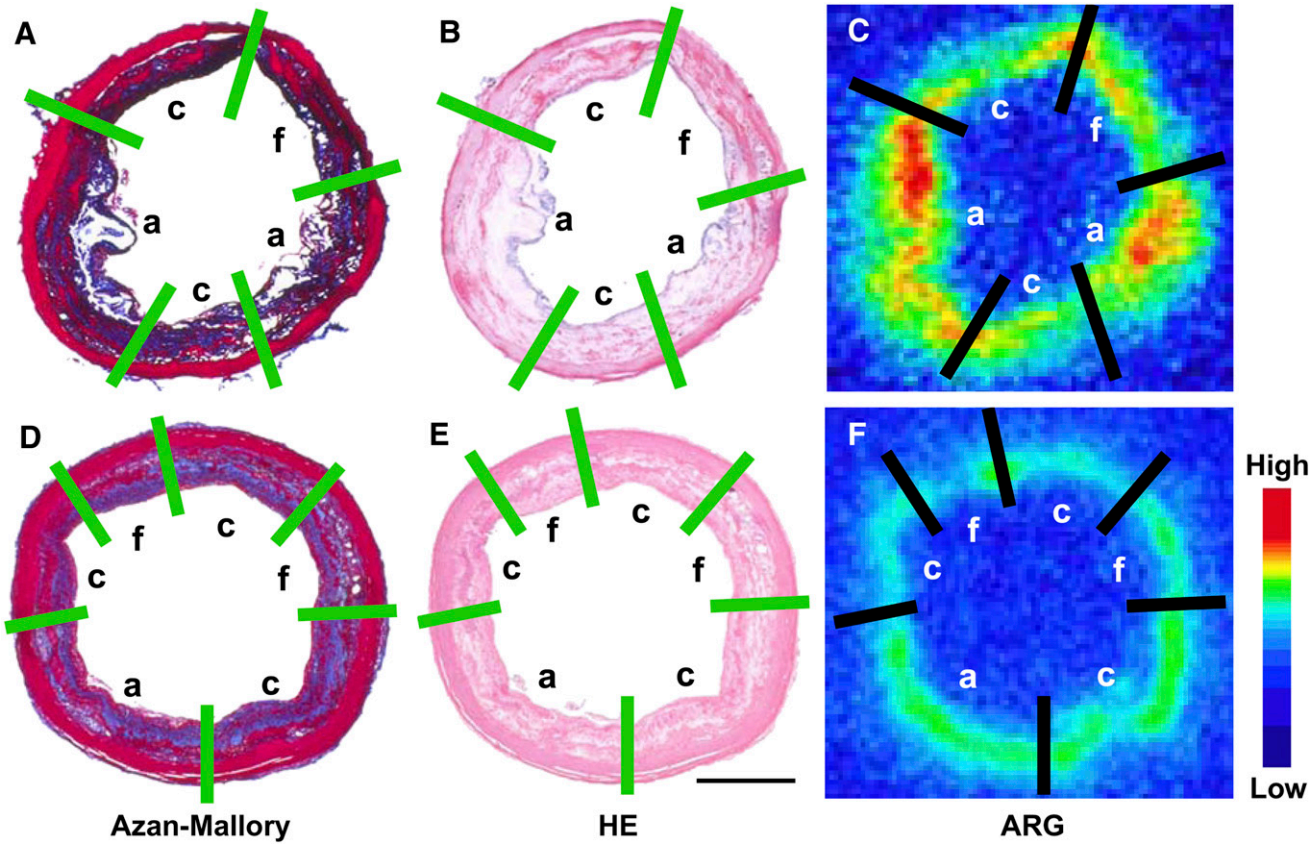

FIGURE 4. Lesion classification scheme in representative photomicrographs and autoradiograms of cross sections of WHHLMI rabbit aortas in ^{99m}Tc-LOX-1-mAb study (A–C) and ^{99m}Tc-IgG2a study (D–F). Atherosclerotic lesions were assigned with AHA classification scheme from Azan–Mallory staining (A and D) and HE staining (B and E) (Fig. 3). Same classification was applied to autoradiograms (ARG) (C and F). ROIs were placed over atherosclerotic lesions in WHHLMI rabbit aortic sections by reference to images with classification scheme from Azan–Mallory staining. a = atheromatous lesions; c = collagen-rich lesions; f = fibroatheromatous lesions. Bar = 1 mm.

Correlation of Regional Distribution of ^{99m}Tc-LOX-1-mAb with LOX-1 Expression

In the ARG studies, heterogeneous ^{99m}Tc-LOX-1-mAb accumulation was observed in the intima of the WHHLMI rabbit aortas, whereas there was little accumulation in the aortas of control rabbits (Figs. 2A and 2B). LOX-1 expression was detected in intimal lesions in WHHLMI rabbit aortas, and the levels of expression differed among the regions (Fig. 2D). As shown in Figures 2B and 2D, higher levels of accumulation of ^{99m}Tc-LOX-1-mAb were observed in regions with high levels of LOX-1 expression, whereas lower levels of accumulation were seen in regions with low levels of LOX-1 expression. Consequently, regional ^{99m}Tc-LOX-1-mAb accumulation in WHHLMI rabbit aortic sections was significantly correlated with LOX-1 expression density ($r = 0.64$, $P < 0.0001$) (Fig. 1). No obvious LOX-1 expression was observed in the aortas of control rabbits (Fig. 2C).

Correlation of Accumulation of ^{99m}Tc-LOX-1-mAb and ^{99m}Tc-IgG2a with Histologic Characteristics

^{99m}Tc-LOX-1-mAb accumulation was dependent on the histologic grade of lesions (Figs. 4C and 6A), and the highest (and significant; $P < 0.0001$) level was seen in atheromatous lesions (type IV), followed in decreasing order by fibroatheromatous, collagen-rich, and neointimal lesions. Figures 6B and 6C show the macrophage density and vulnerability index quantified for each lesion in the ^{99m}Tc-LOX-1-mAb study. The macrophage density and vulnerability index were also the highest in atheromatous lesions, followed in decreasing order by fibroatheromatous, neointimal, and collagen-rich lesions. Consequently, the highest values for ^{99m}Tc-LOX-1-mAb accumulation, macrophage density, and the vulnerability index were observed in atheromatous lesions. In contrast, lower values for ^{99m}Tc-LOX-1-mAb accumulation, macrophage density, and the vulnerability index were seen in collagen-rich and neointimal lesions. Figure 5A shows the regression analysis for ^{99m}Tc-LOX-1-mAb accumulation and the vulnerability index. The regression analysis demonstrated a directly proportional relationship between ^{99m}Tc-LOX-1-mAb accumulation and the vulnerability index ($r = 0.67$, $P < 0.0001$).

In contrast, control tracer (^{99m}Tc-IgG2a) accumulation was independent of the histologic grade of lesions, and the differences among the lesions were not significant (Figs. 4F

TABLE 1
Distributions of ^{99m}Tc-LOX-1-mAb and ^{99m}Tc-IgG2a in Aortic Segments of Control and WHHLMI Rabbits at 24 Hours After Injection

Parameter	Mean ± SD for:		
	^{99m}Tc-LOX-1-mAb in:		
	Control rabbits	WHHLMI rabbits	^{99m}Tc-IgG2a in WHHLMI rabbits
Aortic segment*			
Arch (ascending)	0.45 ± 0.19†	4.0 ± 2.0‡	1.6 ± 0.4†
Thoracic	0.29 ± 0.17†	3.5 ± 1.1‡	1.9 ± 0.3†§
Abdominal	0.29 ± 0.15†	2.3 ± 1.2	1.3 ± 0.6‖
Total	0.32 ± 0.17†	3.2 ± 1.6	1.6 ± 0.5†
A/B ratio	0.12 ± 0.08†	0.69 ± 0.33	0.33 ± 0.11†
A/M ratio	3.1 ± 1.4†	30.8 ± 16.5	18.1 ± 9.8†

*Reported as DUR.
†$P < 0.0001$ vs. WHHLMI rabbits in ^{99m}Tc-LOX-1-mAb study.
‡$P < 0.0001$ vs. abdominal aorta.
§$P < 0.001$ vs. abdominal aorta.
‖$P < 0.05$ vs. WHHLMI rabbits in ^{99m}Tc-LOX-1-mAb study.
Accumulation in each aortic segment was significantly higher in WHHLMI rabbits than in control rabbits. Ascending arch of aorta and thoracic aorta showed higher radioactivity than abdominal aorta in WHHLMI rabbits.

and 6C). The ^{99m}Tc-IgG2a distribution based on the lesion classification was different from that of ^{99m}Tc-LOX-1-mAb, although the distributions of macrophage density and the vulnerability index in the ^{99m}Tc-IgG2a study were similar to those in the ^{99m}Tc-LOX-1-mAb study (data not shown). Furthermore, no correlation between ^{99m}Tc-IgG2a accumulation and the vulnerability index was shown ($r = 0.002$, $P < 0.0001$) (Fig. 5B).

DISCUSSION

There is an urgent need to develop a means to discriminate vulnerable atherosclerotic lesions (atheromatous lesions) from potentially stable lesions in clinical practice, because the disruption of vulnerable plaques causes myocardial and cerebral infarctions. In the present study, we designed and prepared a new imaging agent, ^{99m}Tc-LOX-1-mAb. Our results clearly indicated the potential of ^{99m}Tc-LOX-1-mAb for targeting LOX-1 and evaluating the vulnerability of atherosclerotic lesions.

The immunoreactivity of an agent is an essential factor in in vivo imaging with immunodetection. Flow cytometry analyses indicated that the modification of LOX-1-mAb with the chelating moiety (HYNIC) did not significantly affect the immunoreactivity of the original LOX-1-mAb, although the mean fluorescence intensity was low. Furthermore, ARG and immunohistochemical studies showed that ^{99m}Tc-LOX-1-mAb accumulation in atherosclerotic lesions was well correlated with LOX-1 expression density (Fig. 1). These results suggested the potential of ^{99m}Tc-LOX-1-mAb to specifically recognize LOX-1 in vivo.

The highest level of ^{99m}Tc-LOX-1-mAb accumulation was seen in atheromatous lesions (Fig. 6A) and was significantly correlated with the vulnerability index (Fig. 5A), indicating the ability of this agent to distinguish apparently vulnerable atheromatous lesions from more stable, chronic plaques. This result is consistent with the in vivo relationship between LOX-1 expression and lesion vulnerability (*10*). In contrast, the relationship between ^{99m}Tc-LOX-1-mAb accu-

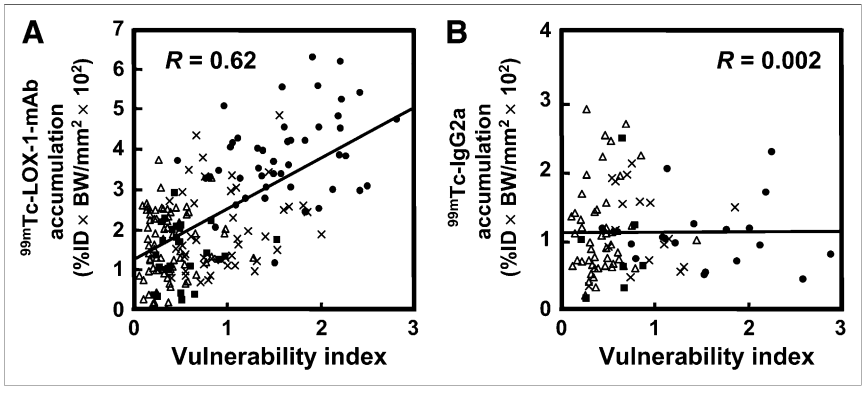

FIGURE 5. Simple regression analyses of vulnerability index with ^{99m}Tc-LOX-1-mAb accumulation (A) and ^{99m}Tc-IgG2a accumulation (B). See legend to Fig. 1 for explanation of units. ● = atheromatous lesion; △ = collagen-rich lesion; × = fibroatheromatous lesion; ■ = neointimal lesion.

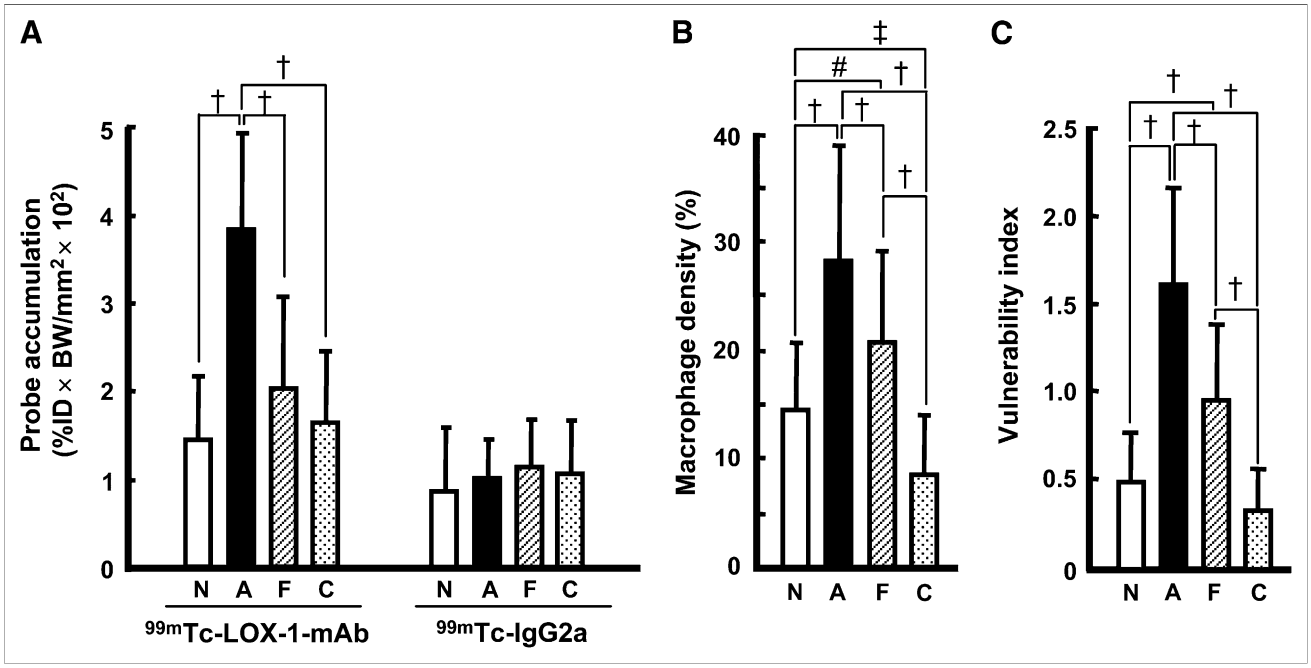

FIGURE 6. Distributions of ^{99m}Tc-LOX-1-mAb and ^{99m}Tc-IgG2a (A) and macrophage density (B) and vulnerability index (C) for each lesion type in ^{99m}Tc-LOX-1-mAb study. Quantitative analysis of autoradiograms provided ^{99m}Tc-LOX-1-mAb and ^{99m}Tc-IgG2a accumulation, expressed as %ID × BW/mm^2 × 10^2 (see legend to Fig. 1 for explanation of units). Data are presented as mean ± SD. $^{\dagger}P < 0.0001$. $^{\ddagger}P < 0.01$. $^{\#}P < 0.05$. A = atheromatous lesions; C = collagen-rich lesions; F = fibroatheromatous lesions; N = neointimal lesions.

mulation (LOX-1 signal) and macrophage density was not high ($r = 0.49$, $P < 0.001$) (data not shown), compared with the relationship with the vulnerability index (Fig. 5A). It has been reported that LOX-1 is intensely expressed in endothelial cells and macrophages (foam cells) in unstable atherosclerotic plaques (*10,27*). In the present study, LOX-1 expression was mainly observed in macrophages; however, LOX-1 was also expressed in endothelial cells and smooth muscle cells. LOX-1 plays multiphasic roles in the formation of vulnerable atherosclerotic plaques (*5–9*). Accordingly, although ^{99m}Tc-LOX-1-mAb accumulation is not highly correlated with macrophage density, ^{99m}Tc-LOX-1-mAb should provide clinically useful information about atherogenesis on the basis of the LOX-1 expression level.

In the present study, we applied a nuclear imaging technique for atherosclerosis imaging. Nuclear imaging is used with the aim of visualizing the biologic properties of atherosclerotic plaques (e.g., cellular composition, inflammatory

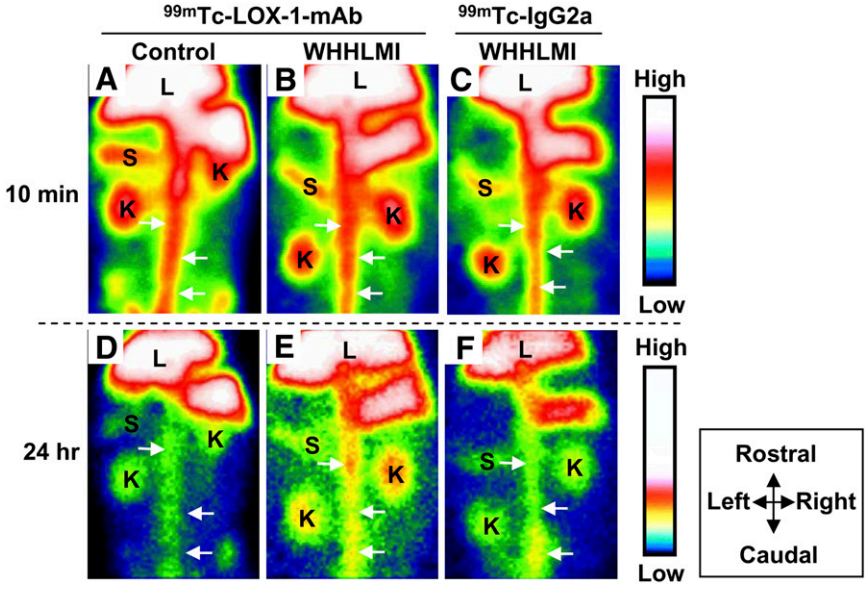

FIGURE 7. Noninvasive imaging of abdominal region with ^{99m}Tc-LOX-1-mAb (A, B, D, and E) and ^{99m}Tc-IgG2a (C and F). Planar images for WHHLMI (B, C, E, and F) and control (A and D) rabbits at 10 min (A–C) and 24 h (D–F) after injection are shown. Field of view = 170 × 120 mm. Arrows = aorta; K = kidney; L = liver; S = spleen.

cell activity, receptor expression, or apoptotic events) (*11,12*). Accordingly, nuclear imaging approaches could provide new diagnostic imaging capabilities for detecting vulnerable plaques on the basis of a specific biologic aspect of atherosclerosis progression. Tsimikas et al. reported the use of a ^{99m}Tc-oxidized LDL–specific antibody for atherosclerosis imaging (*28,29*); this agent allowed the detection of atherosclerosis progression and regression. However, oxidized LDL would need to be injected after the use of this agent to reduce a high level of accumulation of the antibody in the blood and liver. Furthermore, LOX-1 may be a more suitable target than oxidized LDL because it is a specific factor in atherosclerosis progression and is expressed during the early period of atherosclerosis. In contrast, nonspecific uptake into atherosclerosis lesions and high permeability of lesions are important concerns (*30,31*). Therefore, we performed a ^{99m}Tc-IgG2a (control probe) study, which showed the specific uptake of ^{99m}Tc-LOX-1-mAb in atherosclerotic plaques.

As representative nuclear imaging probes, ^{18}F-FDG for imaging metabolic activity in macrophages (*19,32*) and ^{99m}Tc-annexin A5 for imaging apoptosis (*33,34*) were recently used for atherosclerotic plaque imaging. Consequently, it was especially important and intriguing to characterize ^{99m}Tc-LOX-1-mAb in the same animal model (WHHLMI rabbits), focusing on the advantages of ^{99m}Tc-LOX-1-mAb. First, the levels of ^{99m}Tc-LOX-1-mAb accumulation were 2.4- and 3.2-fold higher than the levels of ^{18}F-FDG accumulation (DURs, 1.47 ± 0.90 and 0.72 ± 0.37) in the thoracic and abdominal aortic segments in WHHLMI rabbits, respectively (*19*). Additionally, the level of ^{99m}Tc-LOX-1-mAb accumulation was 5.2-fold higher than the level of ^{99m}Tc-annexin A5 accumulation (DUR, 0.64 ± 0.18 [total aorta]) in aortic segments in WHHLMI rabbits (*33*). These results indicated the potential of ^{99m}Tc-LOX-1-mAb for in vivo imaging, as the accumulation level is an essential factor for this purpose.

Second, ^{99m}Tc-LOX-1-mAb accumulated predominantly in atheromatous lesions. The accumulation ratios of ^{99m}Tc-LOX-1-mAb for atheromatous lesions to other lesions (atheromatous/neointimal, atheromatous/fibroatheromatous, and atheromatous/collagen-rich lesion ratios) were higher than those of ^{99m}Tc-annexin A5 (2.7 vs. 1.3, 1.9 vs. 1.3, and 2.4 vs. 1.8, respectively), indicating that ^{99m}Tc-LOX-1-mAb accumulated more selectively in atheromatous lesions. These results suggested the ability of ^{99m}Tc-LOX-1-mAb to selectively detect vulnerable plaques among heterogeneous atherosclerotic lesions.

In noninvasive imaging studies with ^{99m}Tc-LOX-1-mAb, the atherosclerotic abdominal aorta was imaged more clearly in WHHLMI rabbits than in control rabbits, with decreased blood-pool radioactivity in the abdominal aorta (Fig. 7). This result was confirmed in biodistribution studies (Table 1). However, the difference between control and WHHLMI rabbits seemed to be underwhelming when determined from ARG images, for various reasons. First, the spatial resolution of the SPECT images (6.7 mm at full width at half maximum) was lower than that of the ARG images (50 μm). Second, the A/B ratio in WHHLMI rabbits was 0.69 ± 0.33 at 24 h, indicating that the radioactivity detected by noninvasive imaging was attributable to both aorta and blood radioactivity, although this A/B ratio was comparable to that of ^{99m}Tc-annexin A5 (1.0 ± 0.2 at 3 h after injection). Johnson et al. reported the possibility of in vivo imaging of porcine coronary lesions with ^{99m}Tc-annexin A5 (*35*). However, further studies on the acceleration of clearance of radioactivity from the blood pool are necessary. It has been reported that radiopharmaceuticals derived from low-molecular-weight polypeptides or compounds, small recombinant antibody fragments (Fab and scFv), engineered variants (diabodies, triabodies, minibodies, and single-domain antibodies), and pretargeting antibody methods show rapid clearance of radioactivity from the circulation (*36–38*). The technical progression of SPECT devices could also eliminate the high-background problem.

CONCLUSION

We designed and prepared ^{99m}Tc-LOX-1-mAb for the imaging of LOX-1 and characterized the accumulation of ^{99m}Tc-LOX-1-mAb in atherosclerotic lesions in a rabbit model of spontaneous atherosclerosis. We demonstrated that ^{99m}Tc-LOX-1-mAb could evaluate lesion vulnerability more sensitively than other imaging probes. It could be applied in the clinical setting because of the similarity of the histologic characteristics of atherosclerotic plaques in humans and WHHLMI rabbits. ^{99m}Tc-LOX-1-mAb could be useful as a potential imaging probe for predicting lesions prone to spontaneous rupture and monitoring the effects of timely treatment in patients with advanced atherosclerosis.

ACKNOWLEDGMENTS

This work was partly supported by a Grant-in-Aid for General Scientific Research from the Ministry of Education, Culture, Sports, Science and Technology of Japan and from the Japan Society for the Promotion of Science, by a research grant from the New Energy and Industrial Technology Development Organization (NEDO), by a research grant for cardiovascular diseases from the Ministry of Health, Labor and Welfare (16C-8), and by the 21st Century COE Program "Knowledge Information Infrastructure for Genome Science."

REFERENCES

1. Lendon C, Born GV, Davies MJ, Richardson PD. Plaque fissure: the link between atherosclerosis and thrombosis. *Nouv Rev Fr Hematol.* 1992;34:27–29.
2. Ruberg FL, Leopold JA, Loscalzo J. Atherothrombosis: plaque instability and thrombogenesis. *Prog Cardiovasc Dis.* 2002;44:381–394.
3. Kolodgie FD, Virmani R, Burke AP, et al. Pathologic assessment of the vulnerable human coronary plaque. *Heart.* 2004;90:1385–1391.
4. Sawamura T, Kume N, Aoyama T, et al. An endothelial receptor for oxidized low-density lipoprotein. *Nature.* 1997;386:73–77.

5. Kume N, Kita T. Roles of lectin-like oxidized LDL receptor-1 and its soluble forms in atherogenesis. *Curr Opin Lipidol.* 2001;12:419–423.
6. Moriwaki H, Kume N, Kataoka H, et al. Expression of lectin-like oxidized low density lipoprotein receptor-1 in human and murine macrophages: upregulated expression by TNF-alpha. *FEBS Lett.* 1998;440:29–32.
7. Kataoka H, Kume N, Miyamoto S, et al. Oxidized LDL modulates Bax/Bcl-2 through the lectinlike Ox-LDL receptor-1 in vascular smooth muscle cells. *Arterioscler Thromb Vasc Biol.* 2001;21:955–960.
8. Kume N, Kita T. Apoptosis of vascular cells by oxidized LDL: involvement of caspases and LOX-1 and its implication in atherosclerotic plaque rupture. *Circ Res.* 2004;94:269–270.
9. Li D, Liu L, Chen H, et al. LOX-1 mediates oxidized low-density lipoprotein-induced expression of matrix metalloproteinases in human coronary artery endothelial cells. *Circulation.* 2003;107:612–617.
10. Ishino S, Mukai T, Kume N, et al. Lectin-like oxidized LDL receptor-1 (LOX-1) expression is associated with atherosclerotic plaque instability: analysis in hypercholesterolemic rabbits. *Atherosclerosis.* 2007;195:48–56.
11. Jaffer FA, Libby P, Weissleder R. Molecular and cellular imaging of atherosclerosis: emerging applications. *J Am Coll Cardiol.* 2006;47:1328–1338.
12. Davies JR, Rudd JH, Weissberg PL. Molecular and metabolic imaging of atherosclerosis. *J Nucl Med.* 2004;45:1898–1907.
13. Shiomi M, Ito T, Yamada S, et al. Development of an animal model for spontaneous myocardial infarction (WHHLMI rabbit). *Arterioscler Thromb Vasc Biol.* 2003;23:1239–1244.
14. Eto H, Miyata M, Kume N, et al. Expression of lectin-like oxidized LDL receptor-1 in smooth muscle cells after vascular injury. *Biochem Biophys Res Commun.* 2006;341:591–598.
15. Abrams MJ, Juweid M, tenKate CI, et al. Technetium-99m-human polyclonal IgG radiolabeled via the hydrazino nicotinamide derivative for imaging focal sites of infection in rats. *J Nucl Med.* 1990;31:2022–2028.
16. Ono M, Arano Y, Mukai T, et al. Plasma protein binding of ^{99m}Tc-labeled hydrazino nicotinamide derivatized polypeptides and peptides. *Nucl Med Biol.* 2001;28:155–164.
17. Larsen SK, Solomon HF, Caldwell G, et al. [^{99m}Tc]tricine: a useful precursor complex for the radiolabeling of hydrazinonicotinate protein conjugates. *Bioconjug Chem.* 1995;6:635–638.
18. Ishii K, Kita T, Kume N, Nagano Y, Kawai C. Uptake of acetylated LDL by peritoneal macrophages obtained from normal and Watanabe heritable hyperlipidemic rabbits, an animal model for familial hypercholesterolemia. *Biochim Biophys Acta.* 1988;962:387–389.
19. Ogawa M, Ishino S, Mukai T, et al. ^{18}F-FDG accumulation in atherosclerotic plaques: immunohistochemical and PET imaging study. *J Nucl Med.* 2004;45:1245–1250.
20. Stary HC, Chandler AB, Glagov S, et al. A definition of initial, fatty streak, and intermediate lesions of atherosclerosis: a report from the Committee on Vascular Lesions of the Council on Arteriosclerosis, American Heart Association. *Circulation.* 1994;89:2462–2478.
21. Stary HC, Chandler AB, Dinsmore RE, et al. A definition of advanced types of atherosclerotic lesions and a histological classification of atherosclerosis: a report from the Committee on Vascular Lesions of the Council on Arteriosclerosis, American Heart Association. *Circulation.* 1995;92:1355–1374.
22. Kobayashi S, Inoue N, Ohashi Y, et al. Interaction of oxidative stress and inflammatory response in coronary plaque instability: important role of C-reactive protein. *Arterioscler Thromb Vasc Biol.* 2003;23:1398–1404.
23. Shiomi M, Ito T, Hirouchi Y, et al. Stability of atheromatous plaque affected by lesional composition: study of WHHL rabbits treated with statins. *Ann N Y Acad Sci.* 2001;947:419–423.
24. Mann JM, Davies MJ. Vulnerable plaque: relation of characteristics to degree of stenosis in human coronary arteries. *Circulation.* 1996;94:928–931.
25. Falk E, Shah PK, Fuster V. Coronary plaque disruption. *Circulation.* 1995;92: 657–671.
26. Shiomi M, Ito T, Hirouchi Y, et al. Fibromuscular cap composition is important for the stability of established atherosclerotic plaques in mature WHHL rabbits treated with statins. *Atherosclerosis.* 2001;157:75–84.
27. Chen M, Kakutani M, Minami M, et al. Increased expression of lectin-like oxidized low density lipoprotein receptor-1 in initial atherosclerotic lesions of Watanabe heritable hyperlipidemic rabbits. *Arterioscler Thromb Vasc Biol.* 2000;20:1107–1115.
28. Tsimikas S, Palinski W, Halpern SE, Yeung DW, Curtiss LK, Witztum JL. Radiolabeled MDA2, an oxidation-specific, monoclonal antibody, identifies native atherosclerotic lesions in vivo. *J Nucl Cardiol.* 1999;6:41–53.
29. Tsimikas S, Shaw PX. Non-invasive imaging of vulnerable plaques by molecular targeting of oxidized LDL with tagged oxidation-specific antibodies. *J Cell Biochem Suppl.* 2002;39:138–146.
30. Christensen S, Nielsen H. Permeability of arterial endothelium to plasma macromolecules. *Atherosclerosis.* 1977;27:447–463.
31. Smith EB, Staples EM. Distribution of plasma proteins across the human aortic wall: barrier functions of endothelium and internal elastic lamina. *Atherosclerosis.* 1980;37:579–590.
32. Rudd JH, Warburton EA, Fryer TD, et al. Imaging atherosclerotic plaque inflammation with [^{18}F]-fluorodeoxyglucose positron emission tomography. *Circulation.* 2002;105:2708–2711.
33. Ishino S, Kuge Y, Takai N, et al. ^{99m}Tc-annexin A5 for noninvasive characterization of atherosclerotic lesions: imaging and histological studies in myocardial infarction-prone Watanabe heritable hyperlipidemic rabbits. *Eur J Nucl Med Mol Imaging.* 2007;34:889–899.
34. Kietselaer BL, Reutelingsperger CP, Heidendal GA, et al. Noninvasive detection of plaque instability with use of radiolabeled annexin A5 in patients with carotid-artery atherosclerosis. *N Engl J Med.* 2004;350:1472–1473.
35. Johnson LL, Schofield L, Donahay T, et al. ^{99m}Tc-annexin V imaging for in vivo detection of atherosclerotic lesions in porcine coronary arteries. *J Nucl Med.* 2005;46:1186–1193.
36. Behr TM, Becker WS, Bair HJ, et al. Comparison of complete versus fragmented technetium-99m-labeled anti-CEA monoclonal antibodies for immunoscintigraphy in colorectal cancer. *J Nucl Med.* 1995;36:430–441.
37. Sharkey RM, Karacay H, Cardillo TM, et al. Improving the delivery of radionuclides for imaging and therapy of cancer using pretargeting methods. *Clin Cancer Res.* 2005;11:7109–7121.
38. Sakahara H, Saga T. Avidin-biotin system for delivery of diagnostic agents. *Adv Drug Deliv Rev.* 1999;37:89–101.